

FE Approach to Evaluate the Dynamic Friction Coefficient for the Transient Phase of Rubber-Ice Sliding Interaction

, [Riccardo Leonardi](#)¹, Salvatore Scalera¹, Alessandro Scattina²

¹DYNAmore Italia S.r.l

²Politecnico di Torino, Dipartimento di Ingegneria Meccanica e Aereospaziale

Abstract

The improvement of tractive performance on ice is one of the most challenging aspect in the nowadays tire industry. For this reason, a model which can predict the friction coefficient on ice can be useful in the winter-tire design. However, the highly multiphysics nature of the interaction between rubber and ice [1-4], as well as the magnitude of the dimensions involved make the development of a numerical model a quite complex issue. In this work, a first step for the prediction of the friction coefficient on ice is proposed using the finite element method. The subject of this analysis is the transient phase of the sliding interaction between a rubber block and an ice surface. The *User Define Friction* module of *LS-DYNA* has allowed to implement the suitable friction law for contacts with ice, widely used in the literature [3, 5], which follows a microscopic approach and it is based on a viscous formulation. Considering again the dimensions involved and the duration of the transient phase, it is impossible to directly validate the model through experimental detection [3]. However, in the subsequent steady-state phase, which involves higher amounts of water and longer time, the experimental measurements are easier. To compare the results, in the literature an indirect procedure was used in order to provide a qualitative validation, using the strict link between the transient phase and the steady-state one. The final comparison between the *LS-DYNA* results and the literature results has shown a good correlation level.

1 Introduction

The rubber-ice frictional behaviour is characterized by a series of physical contact phenomena [1]. During the sliding-contact between the rubber and the ice, the frictional heat leads to the melting of the ice. The amount of the water created during the ice melting involves that, among the others friction mechanisms, a viscous formulation has to be adopted to describe the interaction between the two objects [1, 3, 6, 7]. The hydrodynamic effects have also to be considered for a realistic representation of the contact phenomena. In this work, the problem was analysed during the first “transient-phase” of the rubber-ice interaction. During this phase, which endures about 10 *ms*, the micro-mechanical properties of the rubber are fundamental for the determination of the friction coefficient. For this reason, in this work a microscopic approach was used [3]. Figure 1 shows the different length scale for the two approaches considering the same tire contact patch.

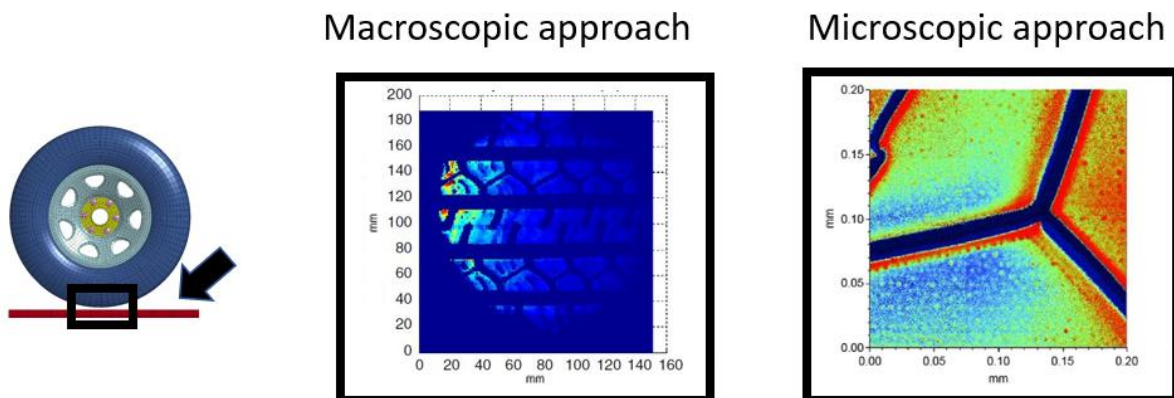


Figure 1: on the left the whole tyre, on the centre the macroscopic approach for the contact patch from [4], on the right the microscopic one from [2]

The friction coefficient between the rubber and the ice is non-stationary during the transient phase. This is mainly due to a succession of different hydrodynamic phenomena. The values assumed by the friction coefficient during this phase significantly affect also the frictional behaviour in the subsequent phase, as shown in figure 2.

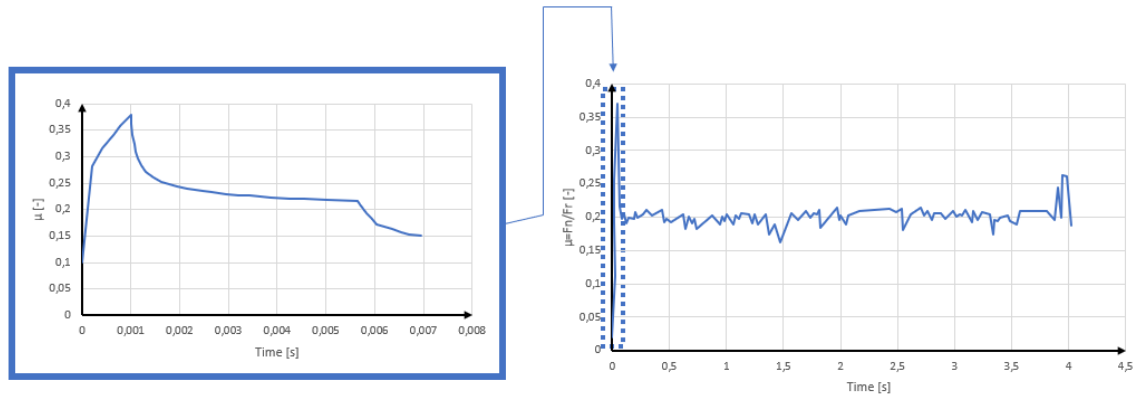


Figure 2: on the left, the transient-phase of the friction coefficient obtained with the LS-DYNA model, on the right experimental measurement of the steady-state phase [3]

In the work of Kessel et al. [5] an analytical solution of the old thermodynamic model was proposed. Wies et al. [3], developed the complete viscous formulation with the addition of the hydrodynamic effects, using the finite element method for the characterization of the micro-mechanical properties of the rubber. In the present work the existing friction condition of a rough rubber block sliding on a smooth ice surface was simulated, following the procedure proposed in [3, 5]. Both the thermodynamic and the hydrodynamic phenomena, as well as the phase change of the ice were considered by directly applying the friction law developed in [3] to a classical thermo-structural simulation, in which the test conditions were replicated. In order to evaluate the friction coefficient, the fluid-structure interaction between the water and the rubber surface has to be considered. However, the dimension of the liquid layer (nanometres) makes impossible to perform a standard CFD analysis, therefore a specific subroutine for the friction coefficient was developed. As discussed in [3], a classical experimental validation procedure is not applicable because, considering the duration of the transient-phase, there is not any existing experimental facility able to measure the ratio between the normal load and the reaction force in such short time period.

Wiese et al. [3], indeed, have proposed an indirect qualitative procedure which is made up by studying the effect of different transient-phase conditions on the subsequent steady-state phase. The comparison between the friction coefficient obtained with the FE simulation developed in the present work and the one proposed in the literature, showed good correlation as discussed in §5. The numerical model developed in this work, is the first step of the ambitious goal of a complete simulation of a full tire model rolling on an icy road.

2 Theoretical formulation

The theoretical formulation implemented in the subroutine comes from [3, 5]. In these works, a viscous formulation for the friction coefficient estimation was developed. A thermodynamic model with smooth surfaces was first considered, the roughness and the related hydrodynamic effects were also included. This section contains a little brief about how this formulation was obtained and an explanation of the considered hydrodynamic effects.

2.1 Thermodynamic formulation

The model initially was made up of a smooth rubber block sliding on an ice surface with a y -velocity v . At the same time the rubber block is also loaded in z -direction with a nominal pressure p_{nom} , as shown in figure 3. A certain amount of water $h_0 = h(t = 0)$ is present at the interface between these two objects since the beginning of the contact between the rubber and the ice. This is due to a molecular interaction phenomenon, called pre-melting [1, 3]. The amount of this initial water layer is quantified experimentally in the literature [1, 3].

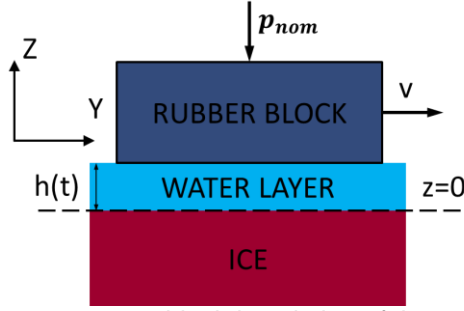


Figure 3: a graphical description of the model

Under these conditions, the thermodynamic balance can be written as in equation (1):

$$\eta_{water} \frac{v^2}{h(t)} = \rho_{ice} L_{ice} \frac{dh(t)}{dt} \cdot \mathcal{X}_{\{T_{ice(0,t)}=T_m\}} + \lambda_{ice} \cdot \partial_z T_{ice}(z, t)|_{z=0} \quad (1)$$

where the frictional energy generated by viscous the shear stress (left-hand side of the equation) is divided in two terms. The two terms are the necessary amount of energy for the melting of the ice and the heat conducted through the ice itself. In particular, the first term on the right-hand side of the equation appears when the temperature of the surface of the ice corresponds to the melting temperature. This condition is represented by the $\mathcal{X}_{\{T_{ice(0,t)}=T_m\}}$ term. This term is equal to 1 when the melting temperature of the ice is reached at $z = 0$ and it is equal to 0 when the temperature is lower than the melting temperature at the same height. From the equation (1), it is simple to obtain the equation for the evaluation of the height of the liquid layer, equation (2):

$$\frac{dh(t)}{dt} = \frac{1}{\rho_{ice} L_{ice}} \left(\eta_{water} \frac{v^2}{h(t)} - \lambda_{ice} \cdot \partial_z T_{ice}(z, t)|_{z=0} \right) \cdot \mathcal{X}_{\{T_{ice(0,t)}=T_m\}}, \quad for \ t > 0 \quad (2)$$

The solution of the equation (2) allows to obtain the friction coefficient. Considering the normal load applied on the rubber block (equation 3) and the reaction (shear) load (equation 4) the Coulomb's friction law described by the equation (5) can be written as in the equation (6).

and that, respectively,

$$F_z = p_{nom} \cdot A_{nom} \quad (3)$$

$$F_{shear}(t) = \tau_{shear} \cdot (t) A_{nom} \eta_{water} \frac{v}{h(t)} \cdot A_{nom} \quad (4)$$

$$\mu(t) = \frac{F_{shear}(t)}{F_z} \quad (5)$$

$$\mu(t) = k \frac{\eta_{water}}{p_{nom}} \frac{v}{h(t)} \quad (6)$$

From the equation (6) is evident as the higher the height of liquid layer, the lower the friction coefficient.

2.2 Thermo-hydrodynamic formulation

As shown in [3], when the rubber block is considered to be rough, additional terms and parameters are added to the equation (2), obtaining the equation (7):

$$\frac{dh(t)}{dt} = \frac{1}{\rho_{ice} L_{ice}} \left(k \eta_{water} \frac{v^2}{h(t)} - \lambda_{ice} \cdot \partial_z T_{ice}(z, t)|_{z=0} \right) \cdot \mathcal{X}_{\{T_{ice(0,t)} < T_m\}} - \frac{8}{3 \eta_{water}} \frac{p_{nom}}{\langle D_{asp} \rangle^2} h_{asp}(t)^3 \cdot \mathcal{X}_{\{H_s(t) < H_V\}}, \quad for \ t > 0 \quad (7)$$

In equation (7) four parameters ($D_{asp}, H_V, H_s(t), k$) were introduced. One additional term $h_{asp}(t)$ was also introduced for modelling the roughness of the rubber and the related hydrodynamic effects. The roughness is modelled as a series of asperities and cavities. Asperities are modelled, as shown in the side section view of the figure 4, as cylinders, following the procedure shown in [3]. The average value of the diameter of these cylinders is indicated by the term $\langle D_{asp} \rangle$. The role of the cavities is to offer an amount of available space for storing the "squeezed-out" water which comes from the liquid layer. With

the variable H_V the average height of the free rubber surface is indicated. Its value is obtained following the experimental procedure indicated in [3]. The average height depends on the micro-mechanical properties of the rubber compound and on the applied normal load.

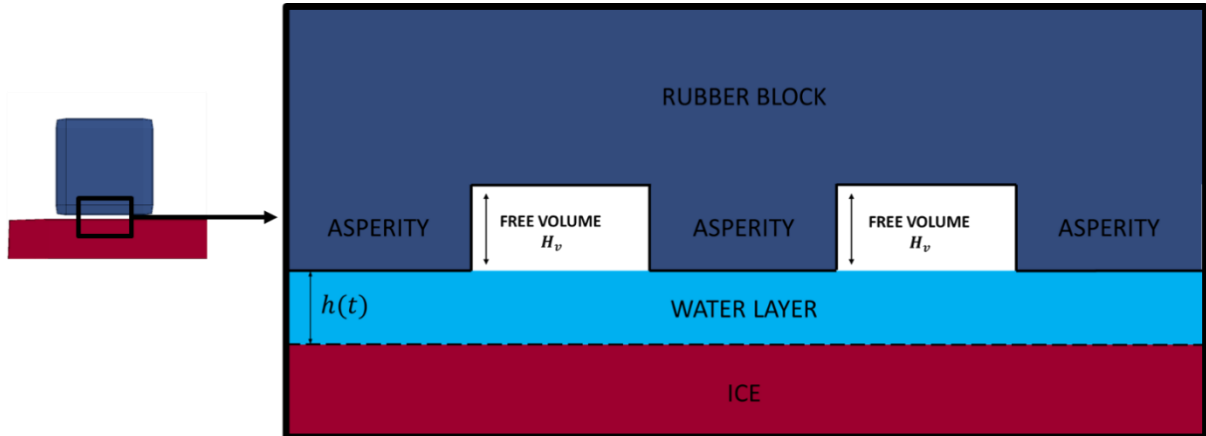


Figure 4: side view of the modelling of the roughness of the rubber block surface

$H_S(t)$ represents the average of the “squeezed-out” water height at time t , evaluated by the equation (8) developed in [3]:

$$H_S(t) = \frac{8}{3 \eta_{water}} \frac{p_{nom}}{\langle D_{asp} \rangle^2} \int_0^t h(t)^3 dt \leq H_V, \quad t \geq 0 \quad (8)$$

Moreover, when the presence of the roughness is admitted, it is necessary to distinguish between the real contact area (sum of all the lower surfaces of the cylinders) and the nominal contact area. For this reason, the relative contact area k , is defined by the equation (9), as indicated in [3]:

$$k = \frac{A_{real}}{A_{nom}} \quad (9)$$

The hydrodynamic contribution to the height of the liquid layer is described by the term shown in the equation (10), obtained in [3]:

$$\frac{dh_{asp}(t)}{dt} = -\frac{8}{3 \eta_{water}} \frac{p_{nom}}{\langle D_{asp} \rangle^2} h_{asp}(t)^3, \quad t > 0 \quad (10)$$

The hydrodynamic effects are the “squeeze-out” effect and the subsequent “saturation” effect. Both of them are described in the following.

2.2.1 Squeeze-out effect

When the asperities of the rubber block transmit the load to the water, a certain amount of the liquid leaves the interface layer, filling the cavities in the rough rubber surface, as shown in figure 5. This phenomenon is called “squeeze-out” effect. The contribution of the squeeze-out effect to the definition of the height of the liquid layer is shown by the equation (10). During the “squeeze-out” effect, a positive behaviour in term of friction coefficient is done by a decreasing trend of $h(t)$, therefore this term has a negative sign

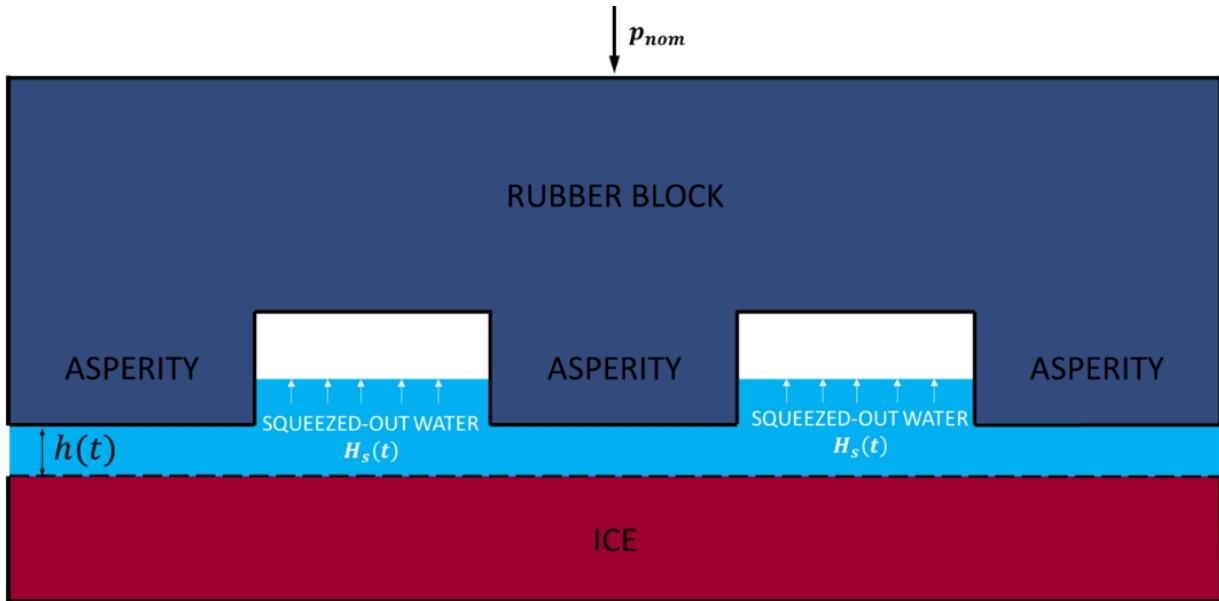


Figure 5: water behaviour during the "squeeze-out" effect

2.2.2 Saturation effect

The water is an incompressible fluid, therefore, when all the cavities are completely filled by the water, no more squeeze-out effect is possible. At this point the saturation effect occurs. A graphical representation of the saturation phenomenon is shown in figure 6. During this phase, the height of the liquid layer increases its value considerably because, on one side the fluid cannot find other ways to escape from the pressure of the asperities and on the other side amount of water is added from the continuously melting process of the ice. This is the worst condition in term of tractive performance of the tyre. This effect can be considered as a "microscopical aquaplaning" effect.

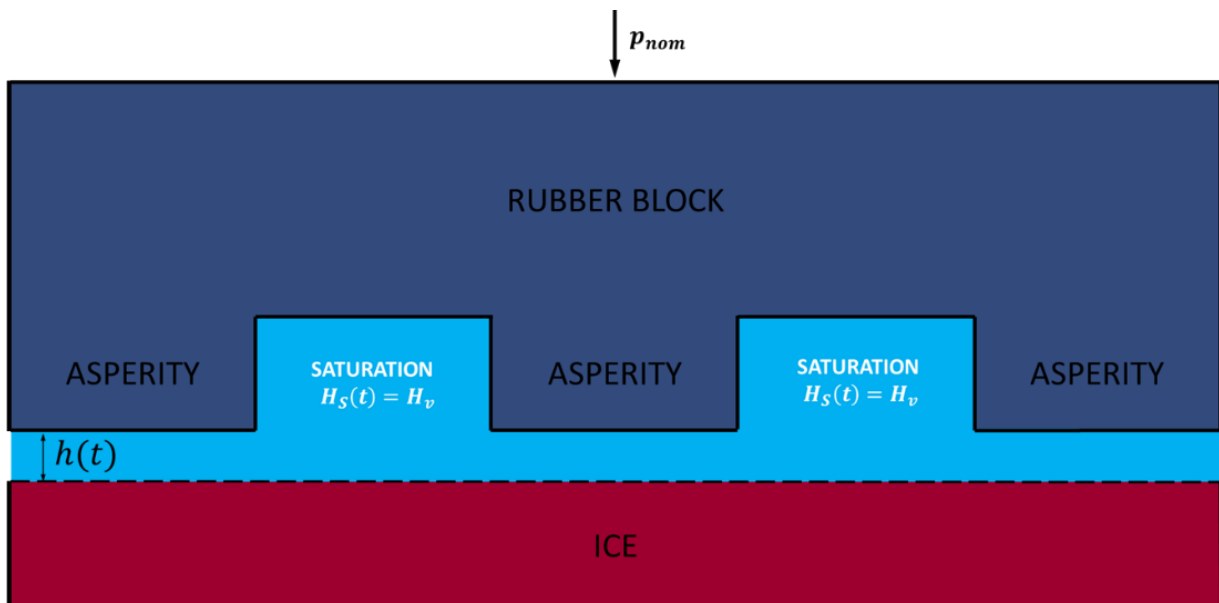


Figure 6: pattern representation of the saturation effect

From a mathematical point of view, the saturation phenomenon means that $H_s(t)$ becomes equal to H_v and then, the $\mathcal{X}_{\{H_s(t) < H_v\}}$ parameter, becomes equal to 0. When the cavities are empty or just partially filled by the water, the $\mathcal{X}_{\{H_s(t) < H_v\}}$ parameter is equal to 1.

3 Numerical solution

The constitutive model was mathematically represented by the equation (7). This is an ordinary differential equation where some terms are not stationary during the time. For this reason, the best way

to find a solution is using a numerical method. Moreover, this is useful for the implementation of the equation in a subroutine. The numerical solution of the equation was developed by splitting the equation (7) in three equations which contain only the active terms.

3.1 Equation set

The equation (7) was divided in three equations (11, 12, 13) dividing the problem along the time in three different phases:

$$\frac{dh(t)}{dt} = -\frac{8}{3\eta_{water}} \frac{p_{nom}}{(D_{asp})^2} h_{asp}(t)^3, \quad for \ t > 0 \quad (11)$$

$$\frac{dh(t)}{dt} = \frac{1}{\rho_{ice} L_{ice}} \left(k \eta_{water} \frac{v^2}{h(t)} - \lambda_{ice} \cdot \partial_z T_{ice}(z, t)|_{z=0} \right) - \frac{8}{3\eta_{water}} \frac{p_{nom}}{(D_{asp})^2} h_{asp}(t)^3, \quad for \ t > 0 \quad (12)$$

$$\frac{dh(t)}{dt} = \frac{1}{\rho_{ice} L_{ice}} \left(k \eta_{water} \frac{v^2}{h(t)} - \lambda_{ice} \cdot \partial_z T_{ice}(z, t)|_{z=0} \right), \quad for \ t > 0 \quad (13)$$

The equation (11) considers the squeeze-out phase, when the temperature on the ice surface is lower than the melting temperature and the cavities are not completely filled by the water. The equation (12) considers the subsequent phase in which the melting temperature of the ice is reached but the cavities are not yet filled. The equation (13) considers the “saturation” effect. A graphical representation of the solution of this equation set is shown in figure 7.

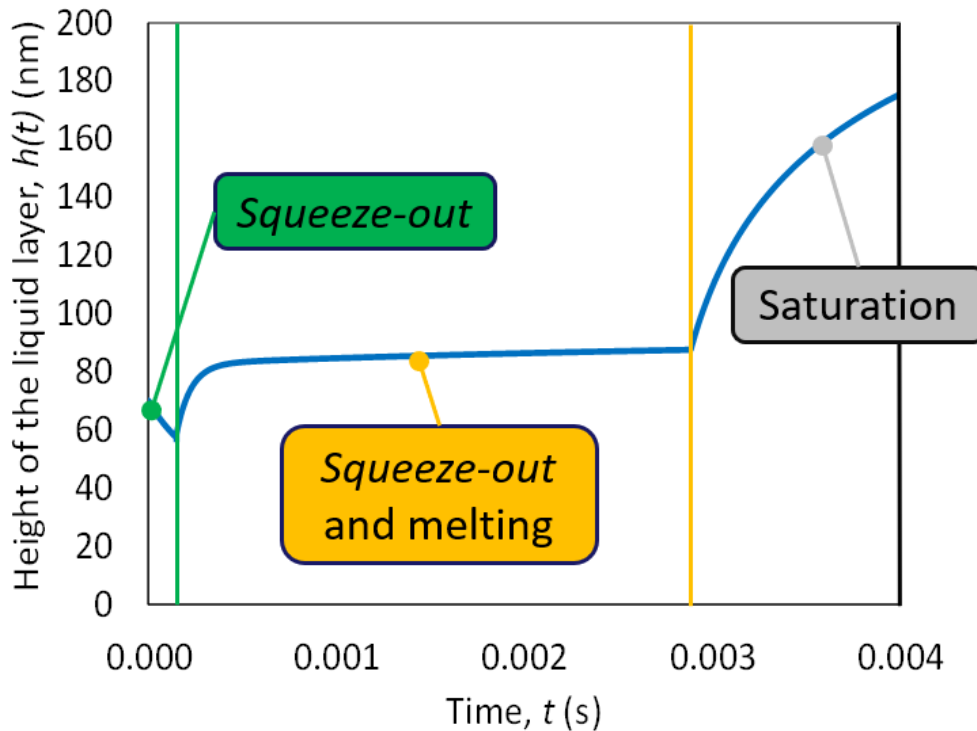


Figure 7: height of the liquid layer as a function of the time, solution obtained from the numerical solution of the equation (7). The three different phases of the phenomenon are shown

3.2 Discretization of the equation set

For the implementation of the equations into a script an explicit method was chosen [9]. Starting from the differential derivative form of the height of the liquid layer it is possible to write the incremental ratio as shown in equation (14)

$$\frac{dh(t)}{dt} = f(t) \rightarrow \frac{h_{j+1} - h_j}{dt} = f(t) + \varepsilon(t) \quad (14)$$

Where the term $\varepsilon(t)$ is the discretization error, dt is the chosen time step and $f(t)$ is the mathematical expression of the derivative. In the first discretization stage the infinitesimal $dh(t)$ is written as a finite difference between the value of $h(t)$ at the time $t + dt$ (called h_{j+1}) and the previous value at the time t (called h_j). With these assumptions it is possible to write the equation (15).

$$h_{j+1} = h_j + dt (f(t) + \varepsilon(t)) \quad (15)$$

Neglecting the discretization error, the value of the parameter, calculated in the next time-step, which represents the solution of the problem is a known entity. This procedure was applied for the solution of the three phases of the equation (7).

3.2.1 Discretization of the squeeze-out phase

The phase 1 is the *squeeze-out* effect and it is modelled with the equation (11). To find the numerical solution of this equation, the terms are associated to the terms in the equation (15) as follow:

- $h_{j+1} = h(t + dt)$
- $h_j = h(t)$
- $f(t) = -\frac{8}{3 \eta_{water}} \frac{p_{nom}}{\langle D_{asp} \rangle^2} h(t)^3$

Hence, neglecting the discretization error, the solution can be written as in equation (16):

$$h(t + dt) = h(t) - dt \left(\frac{8}{3 \eta_{water}} \frac{p_{nom}}{\langle D_{asp} \rangle^2} h(t)^3 \right) \quad (16)$$

The only time-dependent parameter is $h(t)$. For sake of ease, the equation (16) can be in a more compact shape joining together the constant values as shown in the equation (17):

$$h(t + dt) = h(t) - dt (K_3 h(t)^3) \quad (17)$$

where

$$K_3 = \frac{8}{3 \eta_{water}} \frac{p_{nom}}{\langle D_{asp} \rangle^2} \quad (18)$$

For the first step of the simulation the solution is (equation 19):

$$h_1 = h_0 - dt (K_3 h_0^3) \quad (19)$$

Where h_0 is a known value experimentally evaluated as discussed in [3].

3.2.2 Discretization of the squeeze-out and melting phase

The solution of the phase 2 is the most complex as described in section 2. The derivative function for this phase is given by the equation (20):

$$f(t) = \frac{1}{\rho_{ice} L_{ice}} \left(k \eta_{water} \frac{v^2}{h(t)} - \lambda_{ice} \cdot \partial_z T_{ice}(z, t)|_{z=0} \right) - \frac{8}{3 \eta_{water}} \frac{p_{nom}}{\langle D_{asp} \rangle^2} h(t)^3 \quad (20)$$

Solving the heat equation as shown in [5] the equation (20) can be written as the equation (21):

$$f(t) = \frac{1}{\rho_{ice} L_{ice}} \left(k \eta_{water} \frac{v^2}{h(t)} - \lambda_{ice} \cdot \frac{T_m - T_0}{\sqrt{\pi \alpha t}} \right) - \frac{8}{3 \eta_{water}} \frac{p_{nom}}{\langle D_{asp} \rangle^2} h(t)^3 \quad (21)$$

To simplify the derivative expression two terms K_1 (equation 22) and K_2 (equation 23) are introduced.

$$K_1 = \frac{1}{\rho_{ice} L_{ice}} (k \eta_{water} v^2) \quad (22)$$

$$K_2 = \frac{1}{\rho_{ice} L_{ice}} \left(\lambda_{ice} \cdot \frac{T_m - T_0}{\sqrt{\pi \alpha}} \right) \quad (23)$$

K_1 is made up of constant terms, whereas K_2 can be considered as an effective constant value. This condition is true when the solution of the heat equation is obtained considering that the temperature of

the ice will not overcome the melting temperature T_m . Therefore, the equation (21) can be rewritten as the equation (24):

$$f(t) = \frac{K_1}{h(t)} - \frac{K_2}{\sqrt{t}} - K_3 h(t)^3 \quad (24)$$

Consequently, the numerical solution of the equation (12) is (equation 25):

$$h(t + dt) = h(t) + dt \left(\frac{K_1}{h(t)} - \frac{K_2}{\sqrt{t}} - K_3 h(t)^3 \right) \quad (25)$$

The computation of the equation (23) starts when the melting temperature is reached in the thermo-mechanical simulation. Therefore, the first step of the simulation obtained with the equation (21) is (equation 26):

$$h_1 = h_{0m} + dt \left(\frac{K_1}{h_{0m}} - \frac{K_2}{\sqrt{t_m}} - K_3 h_{0m}^3 \right) \quad (26)$$

Where $h_{0m} = h(t_m)$ is the last value obtained by using the equation (16), at the time t_m when the ice starts to melt.

3.2.3 Discretization of the saturation phase

In the last phase the saturation phenomenon is simulated. The expression of the derivative, in this case is (equation 27)

$$f(t) = \frac{1}{\rho_{ice} L_{ice}} \left(k \eta_{water} \frac{v^2}{h(t)} - \lambda_{ice} \cdot \partial_z T_{ice}(z, t)|_{z=0} \right) \quad (27)$$

Solving the heat equation the equation (27) can be written as the equation (28):

$$f(t) = \frac{1}{\rho_{ice} L_{ice}} \left(k \eta_{water} \frac{v^2}{h(t)} - \lambda_{ice} \cdot \frac{T_m - T_0}{\sqrt{\pi \alpha t}} \right) \quad (28)$$

Using the parameters K_1 and K_2 defined above the equation (28) can be written as the equation (29):

$$f(t) = \frac{K_1}{h(t)} - \frac{K_2}{\sqrt{t}} \quad (29)$$

Therefore, the numerical solution of the equation (13) is (equation 30):

$$h(t + dt) = h(t) + dt \left(\frac{K_1}{h(t)} - \frac{K_2}{\sqrt{t}} \right) \quad (30)$$

At this point it is necessary to understand when the saturation effectively occurs. To do this, the numerical solution of the equation (8) was also obtained. In particular, the first step to find the numerical solution was to come-back to a differential equation from an integral formulation as shown in the equation (31):

$$\frac{dH_s(t)}{dt} = \frac{8}{3 \eta_{water}} \frac{p_{nom}}{\langle D_{asp} \rangle^2} h(t)^3 \quad (31)$$

The equation (31) is very similar to the equation used for the phase 1. The derivative function is (equation 32):

$$f(t) = \frac{8}{3 \eta_{water}} \frac{p_{nom}}{\langle D_{asp} \rangle^2} h(t)^3 \quad (32)$$

Applying the explicit method of Euler, the solution of the equation (32) is (equation 33):

$$H_s(t + dt) = H_s(t) + dt \left(\frac{8}{3 \eta_{water}} \frac{p_{nom}}{\langle D_{asp} \rangle^2} h(t)^3 \right) \quad (33)$$

In the equation (33) there is also the constant K_3 . Therefore, the equation (33) can be written in a more compact way (equation 34):

$$H_s(t + dt) = H_s(t) + dt (K_3 \cdot h(t)^3) \quad (34)$$

The calculation for the solution of the equation (34) was made in parallel with the calculation for the solution of the equation (30) because the equation (34) needs the value at the current time-step of $h(t)$. The initial condition for the equation (34) is (equation 35):

$$H_s(0) = 0 \quad (35)$$

The meaning of the equation (35) is that at the beginning of the simulation, the squeeze-out effect is not present. Therefore, during the first step of the simulation, the value of the average height of the squeezed-out water is given by the equation (36):

$$H_{s1} = dt (K_3 \cdot h_0^3) \quad (36)$$

4 LS-DYNA model

The complete LS-DYNA model is made up of two sections which work in parallel [10]. The relationship between these two parts of the model is showed in figure 8.

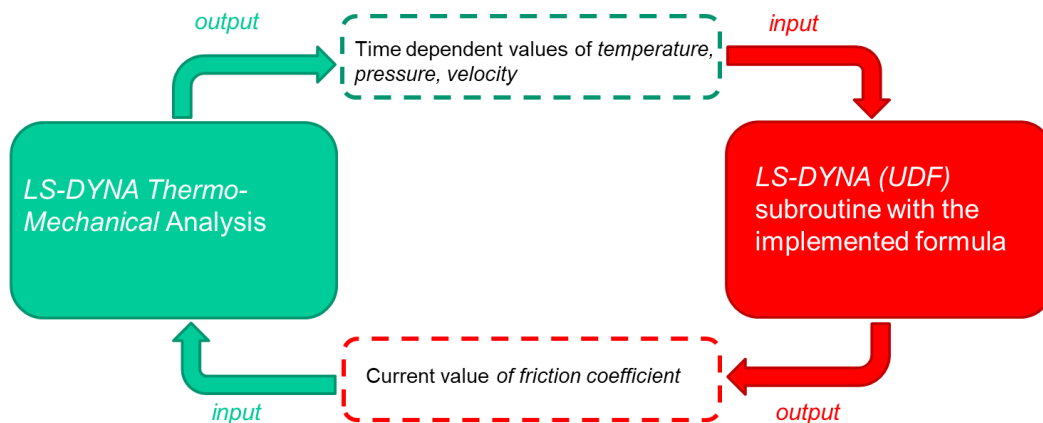


Figure 8: schematic representation of the whole LS-DYNA model, with the loop between the LS-DYNA thermo-mechanical simulation and the customized subroutine for the calculation of the frictional coefficient

Both the two sections of the model are necessary for the calculation of the friction coefficient. The thermo-mechanical section provides all the physical parameters necessary to the algorithm in the subroutine. The subroutine gives as output the value of the friction coefficient at the current timestep which directly affects all the physical parameters of contact. Therefore, the material model and all the physical parameters chosen were the same suggested by Wiese et al. [3]. In the finite element model, the thermo-mechanical analysis is made up of two consecutive phases:

- The pre-load phase, which is performed using the LS-DYNA option called *CONTROL_DYNAMIC RELAXATION [14]. In this phase, the rubber block is loaded by a nominal pressure, then a boundary condition is assigned when the equilibrium is reached. The assigned boundary condition leads the sliding velocity of the rubber block to the desired value. The thermal contribute is neglected during this phase. Consequently, a constant value of the friction coefficient is assumed. For this reason, the subroutine calculation is meaningless because it is switched off in the pre-load phase.
- The transient phase which is the main part of the whole simulation. In this phase, the thermo-mechanical simulation and the *User Define Subroutine* start to work in parallel using the initial condition given by the previous pre-load phase.

The division of the model in two sections is necessary to start the simulation with the same conditions of the test showed in [3] and consequently to compare the resultant friction coefficient. The value of the velocity applied to the rubber block at the beginning of the simulation made in [3] was constant. This condition cannot be imposed as it is in the LS-DYNA simulation because it could create instability due to the high ramp of the velocity applied to the rubber block at the first instant of the simulation. To overcome this problem, a pre-load phase was defined to apply a smooth velocity ramp to the rubber block. Consequently, high peaks of acceleration were avoided.

4.1 Geometry, elements and materials

From a geometrical point of view, the model was defined to reply the physical test conditions described by Wiese et al. in [3]. In particular, the model was made up of two objects:

- The rubber block, with a nominal contact area of 1 mm^2
- The ice block with a longitudinal length (y -direction) sufficient to allow the sliding process at the velocity and for the duration defined in the experimental test.

The figure 9 shows the geometry of the model. The direction of the normal pressure applied on the rubber block is the same of the gravity force ($-z$ axis). The direction of the sliding velocity is along the y axis.



Figure 9: geometry of the LS-DYNA model in its initial condition. The rubber block is in blue whereas the ice block is in red

The LS-DYNA thermo-mechanical analysis needs two different material models for the simulation: a material model for the mechanical part and a material model for the thermal part. To this aim, the material models used in the simulation were:

- The LS-DYNA Mooney-Rivlin material, `*MAT_MOONEY-RIVLIN_RUBBER`, for the rubber block. The same parameters provided by Wiese et al. [3] for the compound B were used.
- The LS-DYNA rigid material, `*MAT_RIGID`, for the ice. The deformation of this part was considered negligible in these load conditions.
- The LS-DYNA thermal isotropic material, `*MAT_THERMAL_ISOTROPIC`, for both ice and rubber. This is the simplest thermal material model available in LS-DYNA. It was chosen considering the thermal parameters available for the rubber and for the ice [8].

Different choices were also made in the element formulation for the ice block and for the rubber block, in order to improve the accuracy of the results and to reduce the calculation time. In particular:

- For the rubber block, a tetrahedral formulation with one point of integration was adopted. This choice was made considering the high level of deformation under the sliding condition. The idea was to take advantage of the numerical limits of this kind of elements. It is well known as the tetrahedrons are more rigid than the other elements [10]. This condition was used to overcome numerical problems which frequently occur during the sliding simulation.
- For the ice block, the hexahedral elements with a fully-integrated formulation was used.

5 Results and discussions

The trend of the friction coefficient shown in Figure 10 put in evidence the three different phases:

- Phase 1: it is mainly governed by the squeeze-out effect
- Phase 2: it starts with a singularity point when the melting temperature is reached. The increase of temperature produces additional water leading to an increasing value of the height of the liquid layer $h(t)$
- Phase 3: it is governed by the saturation effect

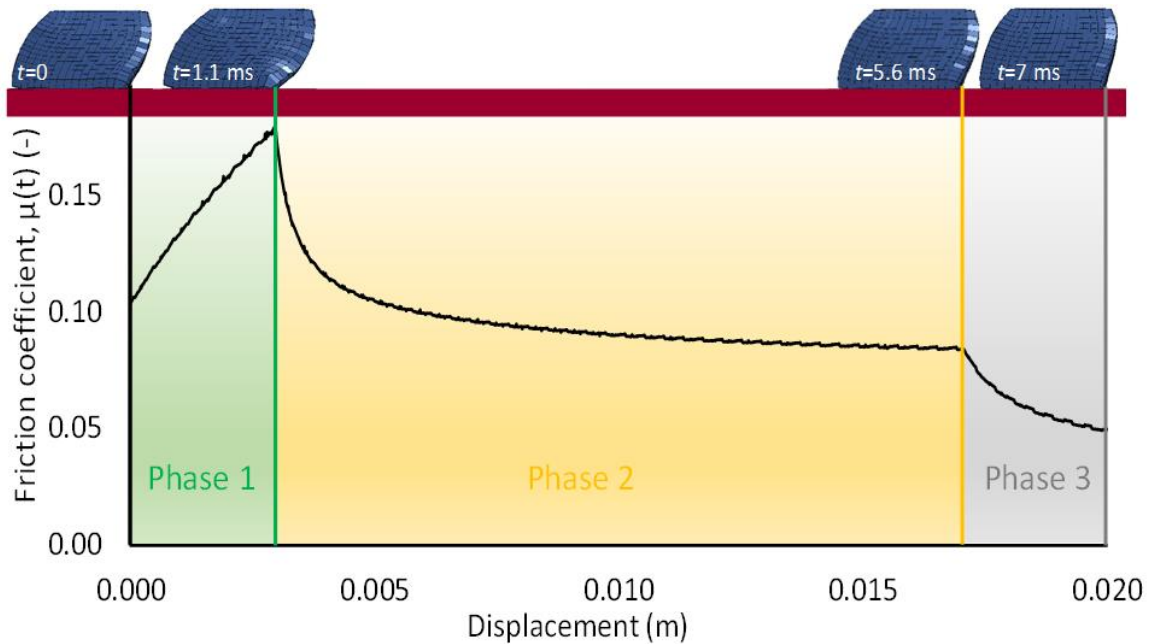


Figure 10: trend of the friction coefficient obtained with the numerical model as a function of the sliding of the rubber block. In the top part of the figure it is possible to appreciate the deformation of the rubber block at the beginning of the different phases.

The comparison between the numerical results obtained with LS-DYNA and the results proposed in literature [3] shows that (Figure 11):

- a good level of agreement is obtained in particular when the pressure applied on the rubber block is low (Figure 11a)
- the differences related to the melting-time, in particular when the pressure is high, are due to the uncertainty about the thermal parameters of the rubber material (Figure 11b)

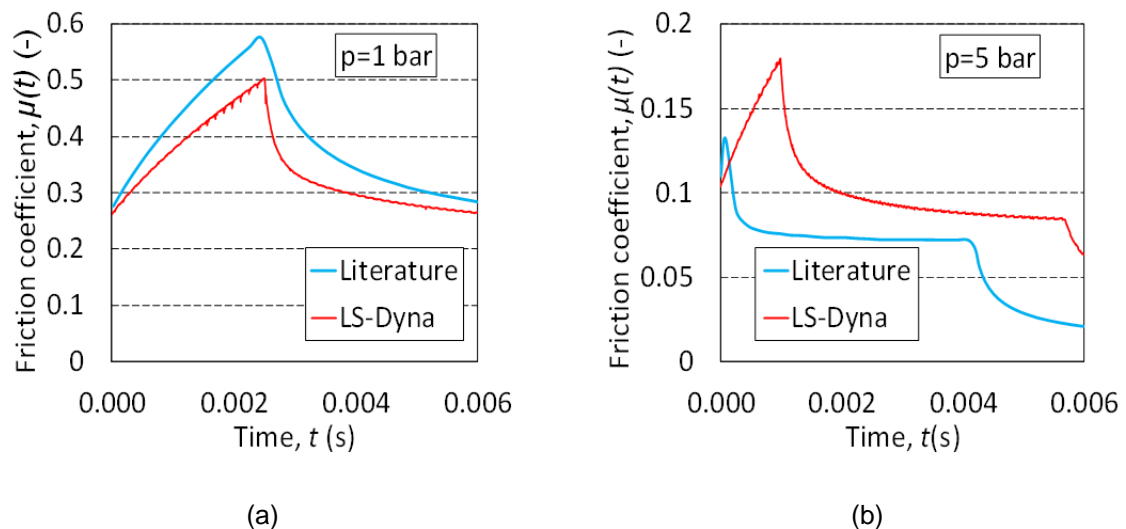


Figure 11: comparison between the numerical results obtained with LS-DYNA and the results proposed in literature

The absolute value of the friction coefficient was in good agreement with the paper result [3] in particular when the nominal pressure is 1 bar. The time at which the melting temperature was reached is also very similar (about 2.5 ms). At this time, the peak of the friction coefficient obtained with the LS-DYNA simulation was 0.51 whereas in the paper it was about 0.55.

The general trend of the curves is also very similar. The uncertainty on the material parameters led to a short anticipation on the time at which the melting temperature is reached. This means that, the absolute value of the friction coefficient will be lower.

Some more differences were obtained when the higher nominal pressure (5 bar) was applied. The melting temperature was reached with a delay of 1 *ms* respect to the results obtained by Wiese et al. [3]. This delay affects also the absolute maximum value of the friction coefficient obtained in the LS-DYNA simulation, which is higher than the one obtained in [3]. This difference was due to the squeeze-out phase which had a longer duration. The reasons of these differences are mainly due to the uncertainty about the correct value of the thermal parameters of the ice and of the rubber. Moreover, the material model adopted in the simulation does not take into account the viscoelastic effects of the deformation of the rubber. The uncertainty on the material parameters influenced the timing of the simulation in a similar way for the nominal pressure of 1 bar. The effect of the time-delay, with a different melting time lead to a different saturation time, therefore the absolute value of the friction coefficient had a certain level of discrepancy.

6 Summary

In this work, the transient phase of the rubber-ice sliding contact was studied from a microscopic point of view. This allowed to catch the dynamic behaviour of the friction coefficient during this phase, due to the melting of the ice and the related hydrodynamic phenomena. The dimension involved does not allow the direct simulation of the thin water layer. A customized subroutine was developed with the viscous formulation of friction developed in [3]. A simulation in which the viscous effects were taken into account was performed with the subroutine. The validation of the model was carried out comparing the LS-DYNA results and results present in the literature [3]. because the duration of the simulation and the magnitude of the others parameters are prohibitive to be measured with a laboratory tests, A good correlation level was obtained even if some melting-delay was obtained for the simulation with higher nominal pressure (5 bar).

7 Literature

- [1] Persson BNJ. Theory of rubber friction and contact. *J Chem Phys* 2001;115 (8):3840–61.
- [2] Tuononen, A. J., Kriston, A. & Persson, B. Multiscale physics of rubber-ice friction. *The J. Chem. Phys.* **145**, 114703 (2016).
- [3] C. Klapproth, T. M. Kessel, K. Wiese, and B. Wies, “An advanced viscous model for rubber–ice-friction,” *Tribol. Int.* **99**, 169–181 (2016).
- [4] A. K. Bhoopalam, C. Sandu, and S. Teheri, “A tire-ice model (TIM) for traction estimation,” *Journal of Terramechanics* **66**, 1–12 (2016).
- [5] Kessel TM, Mundl R, Wies B, Wiese K. An analytical thermodynamical approach to friction of rubber on ice. *TireSciTechnol*2012;40(2):124–50..
- [6] B.N.J. Persson, E. Tosatti: The effect of surface roughness on the adhesion of elastic solids, *J. Chem. Phys.* **115**, 5597–5610 (2001).
- [7] Scaraggi M, Persson BNJ. General contact mechanics theory for randomly rough surfaces with application to rubber friction.
- [8] The Engineering ToolBox <http://www.engineeringtoolbox.com/ice-thermal-properties-d_576.html>.
- [9] C. Canuto, *Modelli e Metodi Numerici*-2013.
- [10] LS-DYNA Manual R10.0 Vol I, Vol II